FIBER OPTICS

1. Introduction

Optical communication was long considered as a possibility for high speed data transmission because light at terahertz frequency is capable of enormous bandwidth. The power of lightwave communication could not be tapped, however, until the obstacle of a suitably transparent transmission medium was overcome.

For example, in 1880 Alexander Graham Bell patented the photophone, a device that utilized the atmosphere as a transmission medium. Here a narrow beam of sunlight was focused on a thin mirror, soundwaves produced by the human voice caused the mirror to vibrate, and the light was transmitted to a selenium detector. The resistance of the selenium varied proportionally, producing a current variation in the receiver that was akin to speech waves. The transmission distance limit of the system is dependent on the loss encountered along the transmission path, combined with the brightness of the light source and the sensitivity of the detector. In the case of the photophone, disruptions from rain, fog, smoke, clouds, and other atmospheric disturbances severely limited the maximum distance.

The invention of the laser in 1958 prompted the beginning of the story of optical fiber communications. This device was capable of producing a high intensity, coherent beam of light which could be modulated at a high rate (see LASERS). Still, no transmission medium of suitable clarity was available. A number of sophisticated systems for transmitting light signals were produced (1,2) using a closed system of pressurized aluminum pipes, thus solving the problem of opacity caused by atmospheric disturbances. However, the use of lenses to control beam divergence introduced reflection losses that limited the range of such systems. Lens losses were minimized upon the invention of a gas lens (3) created by uniform heating of the gas in the tube, forming a density and therefore a refractive index gradient in the gas to focus the beam. Although this system worked well, systems of buried metal pipes were expensive and could only be economical for very wide band communications networks. The need was evident for a low loss transmission medium which could be produced in long lengths at a reasonable cost.

Transmission of light through thin glass fibers was proposed in the 1960s (4). However, at that time no glass (qv) existed with optical absorption sufficiently low to be practical. In addition to low loss transmission, the light must be guided by a refractive index structure such that a cylindrically symmetric composite, having a core of higher refractive index than the surrounding cladding, confines the light by the process of total internal reflection. It was predicted that losses of less than 20 dB/km could be achieved in glass if transition metals, initially present in the starting materials or added during processing, could be limited to a level of ca 1 ppm. Strides in reducing impurities and fabricating waveguide structures by a variety of methods were made to the point where by the mid-1980s, near-intrinsic optical losses in silica glass were achieved. During this same period the guiding properties in lightguides were improved to realize the high bandwidth capability of the medium. The number of voice channels available has also increased dramatically as higher bit-rate systems are manufactured to use more of the fiber's potential bandwidth. These systems are limited more by the electronics driving the laser sources than by the properties of the glass fiber used to transmit the signal. This limitation has precipitated the development of a new generation of fiber-optic systems where the glass fiber, once solely a passive component, is becoming an active amplifying component. Rare-earth-doped fibers are being manufactured for use in optical amplifiers. When pumped by light of an appropriate wavelength, an optical signal triggers emission at the signal wavelength, resulting in amplification.

In early telephones, sound (voice) waves caused a carbon microphone's resistance to vary, thus varying the current flowing in a series external circuit. This d-c current could then be used to regenerate voice waves in a receiver. Two wires were required to carry a single conversation. With time, telecommunications traffic was encoded on a-c carriers, at first using amplitude or frequency modulation, and more recently pulse code modulation.

The growth in the number of circuits necessary to meet the growing demand for capacity prompted the use of ever higher carrier frequencies to increase capacity. This advance was limited by two obstacles. First, the resistance of the wire increases with higher frequencies, as current is carried on a thinner and thinner surface layer of the metallic conductors. Second, noise becomes incorporated onto the signal during analogue transmission and results in both degradation and distortion of the signal. The problems generated by the use of higher carrier frequencies were initially circumvented by the use of single-sideband microwave radio links. These systems first operated from towers spread across the continent and then from Telstar and other satellites which provided up to 1800 voice circuits when operated at 4 GHz (4×10^9 cycles per second). The use of radio was eventually limited by the allocation of suitable frequencies.

The development of digital encoding solved the problem of signal degradation noise. Using this method, the amplitude of an analogue waveform is sampled at frequent intervals and coded into a binary (0s and 1s) sequence of digits. A voice waveform requires the transmission of 64,000 bits/s, which are digitally transmitted by a series of positive and negative electrical pulses. The optical equivalent uses pulses of light transmitted over glass fiber. Unlike the electrical signal, laser light may be modulated at a frequency high enough (10s of gigahertz) for any conceivable communication need.

Figure 1 gives a comparison of analogue and digital transmission schemes. The incoming signal (Fig. 1**a**) can be transformed directly into an intensity
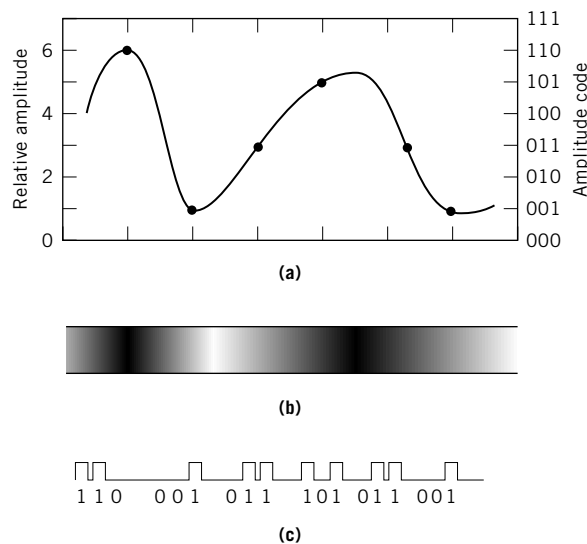

Fig. 1. (**a**) A transmission signal and its (**b**) analogue and (**c**) digital encoding.

variation of the light beam (Fig. 1**b**). A photodetector at the receiver converts this varying intensity into an electrical signal which is then amplified to reproduce the original waveform. Such a signal becomes increasingly degraded and distorted during transmission and amplification. Improved fidelity is provided by digital encoding (Fig. 1**c**). In the digital scheme the signal is encoded by flashes of light at regularly timed intervals. The sampling rate must be twice that of the highest frequency component for accurate representation of the waveform. A voice signal having a maximum frequency of 4000 Hz must be sampled at a rate of 8000/s. The binary coding of 0s and 1s corresponds to the absence and presence of light. Representation of the height of a voice waveform requires eight bits (a bit is a 0 or a 1). Therefore, to sample a voice wave for one second the digital system requires 64,000 bits ($8,000$ samples $\times$ 8 bits/sample). Although the intensity of the light signal diminishes over distance, as long as it remains above the threshold of the detector the signal can be cleanly regenerated because a pulse is either present or absent. In this manner, noise is eliminated.

2. Principles of Light Guidance

Light guidance is governed by the structure of the lightguide itself. The refractive index, n, of a material is defined as the ratio of the speed of light in a perfect vacuum to the speed of light through that material. This property is a function of both the composition of the material and the wavelength of the transmitted light. The higher the refractive index of a material, the more light is retarded, or slowed, in passing through it. At the interface of two materials of different refractive indexes, light is refracted, or bent toward the higher index medium by an angle the sine of which is proportional to the relative indexes of the two media. This property is known as Snell's law. Light that travels in a medium of higher refractive index at an angle less than the critical angle, $_c$, is totally reflected. This property of total internal reflection provides a means to transmit light over long distances without radiative losses.

The ability of a waveguide to collect light is determined by the numerical aperture (NA) which defines the maximum angle at which light entering the fiber can be guided.

$$\mathrm{NA} = \sin\theta_c = \left(n_1^2 - n_2^2\right)^{1/2} - n_1(2\Delta)^{1/2} \tag{1}$$

where

$$\Delta = (n_1 - n_2)/n_1 \tag{2}$$

and typically $\Delta \ll 1$; n_1 is the refractive index of the core; and n_2 is the index of the cladding. Lightguide structures are shown in Figure 2. Whereas Figures 2**a** and 2**b** are multimode structures having relatively higher Δs and core diameters on the order of 50 μm, Figure 2**c** is a single-mode fiber of lower refractive index and a core diameter < 10 μm. The number of modes that can propagate in a fiber is governed by Maxwell's equations for electromagnetic fields, and is related to a
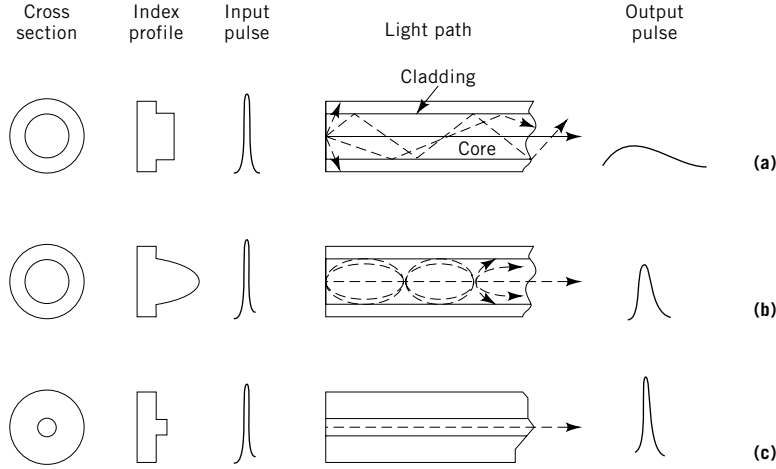
Fig. 2. Types of optical fiber: (**a**) multimode stepped index, (**b**) multimode graded index, and (**c**) single-mode stepped index.

dimensionless quantity V called the normalized frequency:

$$V = (2\pi a/\lambda)\mathrm{NA} \simeq (2\pi a n_1/\lambda)\,(2\Delta)^{1/2} \tag{3}$$

where λ is the wavelength of light in vacuum and a is the radius of the fiber core. For example, as the core becomes smaller, there are fewer paths for the light to undergo total internal reflection. When V is less than 2.405 for a stepped index core profile only a single mode of light, the fundamental mode, can propagate. All other modes are cut off. This governs the design of single-mode fibers as shown in Figure 2**c**.

2.1. Attenuation.   The exceptional transparency, or low attenuation, of silica-based glass fibers has made them the predominant choice for optical transmission because of the low level of absorption and scattering of light as it traverses the material. Together these comprise optical attenuation, or loss, measured in dB where

$$\mathrm{loss}\ (\mathrm{dB}) = 10\log(I_0/I) \tag{4}$$

I_0 is the input intensity and I is the output intensity. Values for loss are typically given per kilometer of fiber. The window of transparency for silica-based glass, shown in Figure 3, is bounded at short wavelength because of electronic transitions. At longer wavelengths molecular vibrations cause attenuation. Between these two regions is the transmission window in which the attenuation is limited mainly by Rayleigh scattering. The ultraviolet absorption edge is determined by the electronic band gap of the material. It decays exponentially with increasing wavelength and becomes negligible at infrared wavelengths. Rayleigh scattering results from glass composition and density fluctuations on a scale shorter than the wavelength of light. These losses decrease as the fourth power of the wavelength of light ($\alpha\lambda^{-4}$). Extrinsic loss mechanisms, such as absorption caused by
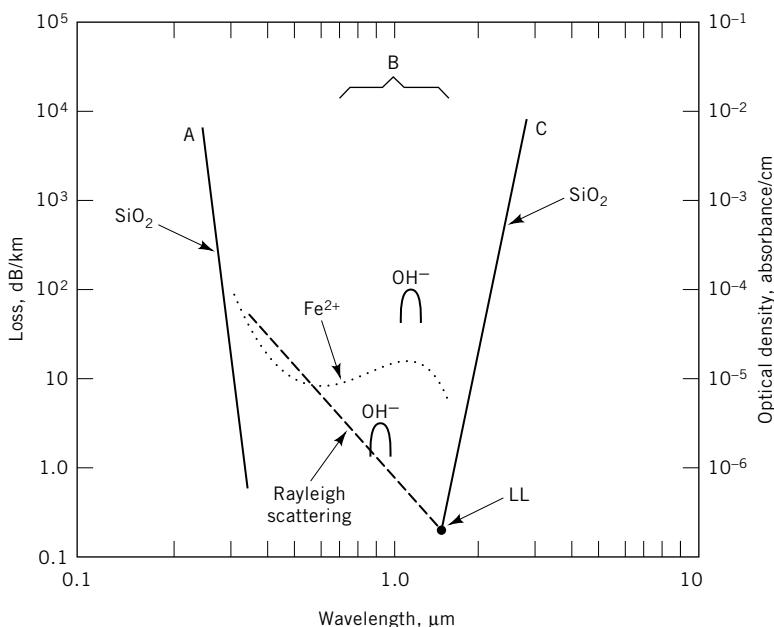
Fig. 3. Transmission profile for a silica-based glass fiber. Region A represents electronic transitions; B, the transmission window; and C, molecular vibrations. Point LL is the lowest loss observed in an optical fiber. Absorption profiles for (——) OH⁻ and (···) Fe²⁺ are also shown. See text.

transition-metal or hydroxyl ion, OH^-; contamination, may dominate over Rayleigh scattering in the transmission window of interest. At longer wavelengths absorption arises from oxygen-cation multiphonon vibrational modes in the glass lattice.

Additional optical attenuation may result from large-scale imperfections or defects in the glass structure as well as waveguide imperfections formed during processing of the glass. Fluctuations longer than the wavelength of light, such as diameter variations, may cause Mie scattering. Even in a nearly perfect glass, absorptions from low level cation impurities, eg, on the order of 1 ppm as shown in Figure 3, are detrimental. Similarly, point defects in the anion network can play a role in controlling loss; suboxides of germanium can be formed at high temperature in an oxygen-deficient reaction and result in coloration, especially after exposure to radiation (5). If these extrinsic losses are avoided, as is typical of current production, then fiber attenuation is dominated by Rayleigh scattering and decreases as λ^{-4} until the multiphonon edge is intersected. The lowest loss for SiO_2 glasses is thereby achieved between 1.3 and 1.55 μm, although the OH^- overtone absorption at 1.38 μm often limits loss around that wavelength. Even for low attenuation, system performance was limited by pulse broadening or dispersion effects and designers generally exploited the shorter wavelength side of the curve because chromatic dispersion can be made zero at 1.3 μm. However, by proper fiber design the minimum dispersion can be shifted to 1.55 μm where higher transparency is advantageous for long-distance transmission.

   2.2. Dispersion.   The effects of dispersion on the ultimate system perfor-
mance are as important as the attenuation. Dispersion arises from the variation
of the velocity of light with the wavelength of the light. Two types of dispersion
which occur are intermodal, found only in multimode fibers, and chromatic,
which is important for single-mode performance. Intermodal dispersion relates
to the delay differences experienced by modes traveling in different regions of
the waveguide. For example, the fundamental mode travels in a straight path,
whereas higher order modes travel a helical route (Fig. 2**b**). To minimize this
effect, multimode fibers are designed having refractive index gradients such
that the lower order modes are more heavily retarded by higher index glass
at the center of the core. A minimum in intermodal dispersion is achieved
when the index distribution varies as $n_1[1 - \Delta(r/a)^\alpha]$, where n_1 is the refractive
index of the core; Δ is the relative index difference; r is the radial position at
which the calculation is made (at the outer edge of the core $r = a$; in the center
$r = 0$); a is the core radius; and α, the profile coefficient, is approximately 2. The
optimum value for α is wavelength- and compositionally dependent.

   In single-mode fibers intermodal dispersion is not a factor; however, pulse
broadening occurs owing to chromatic dispersion. Optical sources are not spec-
trally pure and typically emit light over a narrow range of wavelengths. The
speed of light, controlled by the refractive index, is dependent on wavelength,
and slightly different wavelengths travel at different velocities because of two
effects: material dispersion and waveguide dispersion. Fortuitously, as can
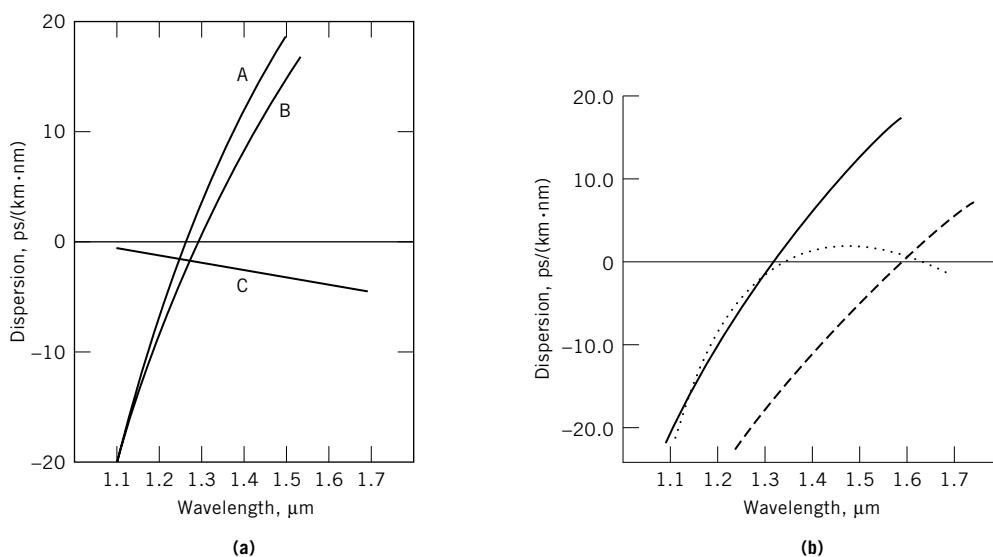be seen in Figure 4**a**, these effects are opposite in sign and may be cancelled.

Fig. 4.   (**a**) Types of dispersion: A, material; B, total chromatic; and C, waveguide.
(**b**) Dispersion in single-mode lightguides where (—) corresponds to a 1.3 μm operation
having a profile of (⊓); (– – –); to a dispersion shifted smaller core higher index system
having a (⊓ ⋀) profile; and (⋯) to an ultrabroad band of more complex structure
(+⌐⊓⊓⌐+).

Material dispersion, which is essentially independent of the fiber's structure or, for high silica glasses, its glass composition, is a nonlinear property and rises steeply with wavelength. Waveguide dispersion, controlled by the fiber design, can be optimized to cancel material dispersion. For waveguide designs, where the glass consists primarily of silica doped with small amounts of other ions, the zero dispersion cross-over occurs near 1.3 µm.

Waveguide dispersion depends on how much of the power travels in the cladding of the fiber relative to the amount traveling in the core. Proper design of the fiber's core diameter and refractive index profile may be fine-tuned to completely cancel the material dispersion at a given wavelength, or to flatten the total dispersion over a range of wavelengths (6). In Figure 4**b** the relationship between fiber profile and waveguide dispersion is illustrated. The shift to longer wavelength operation to take advantage of lower optical losses has led to more complex designs, as seen in the dotted curve where the zero dispersion crossover occurs at two wavelengths of low loss in the fiber allowing multichannel operation at both 1.3 µm and 1.55 µm in a single fiber.

3. Optical Fiber Fabrication

Viable glass fibers for optical communication are made from glass of an extremely high purity as well as a precise refractive index structure. The first fibers produced for this purpose in the 1960s attempted to improve on the quality of traditional optical glasses, which at that time exhibited losses on the order of 1000 dB/km. To achieve optical transmission over sufficient distance to be competitive with existing systems, the optical losses had to be reduced to below 20 dB/km. It was realized that impurities such as transition-metal ion contamination in this glass must be reduced to unprecedented levels (see Fig. 4).

3.1. Double Crucible. The earliest attempts at producing high purity glass employed the double crucible technique. Low optical losses were achieved by purifying the starting materials to a high degree and taking care not to contaminate them during the forming process (7,8). Soda lime silica glasses and sodium borosilicate glasses were prepared from materials purified to parts per billion levels of transition metals. The methods used in the purification included solvent extraction, recrystallization, ion-exchange, and electrolysis. After the bulk material was melted and fined, a process by which gas is removed from the melt to minimize bubble formation, it was drawn into cane. This cane was then fed to a continuous casting system of concentric platinum crucibles. The glass for the core was fed into the inner crucible, exiting as a thin glass stream which entered the second crucible where it was coated with glass of a different composition (lower index) to make a guiding structure. By controlling the draw rate, ionic diffusion between the glasses in the lower crucible produced the gradient in the refractive index necessary to minimize intermodal dispersion.

In spite of the elegance of this technique, contamination occurred during processing, leading to impurity levels in the glass on the order of parts per million rather than the ppb levels necessary. Many ingenious methods were devised in an attempt to eliminate these impurities. The most successful of these used control of the oxygen partial pressure of the processing atmosphere during

manufacture. Absorption owing to two principal contaminants, iron and copper, could be reduced by altering the valence state. The iron could be oxidized to the Fe^{3+} and copper reduced to Cu^+, diminishing the strong absorptions in the near-ir by Fe^{2+} and Cu^{2+}.

The best fibers, installed in systems operating at 0.9 µm, had losses of 5 dB/km. The lower intrinsic losses in the 1.3 to 1.55-µm window were unattainable by this technique. Fundamental cation−oxygen vibrational modes as well as OH^- contamination were intrinsic to the compositions.

High silica glasses having lower losses at wavelengths from the visible to the infrared became available through technology using vapor-phase techniques where silicon tetrachloride [10026-04-7], $SiCl_4$, is the precursor to silicon oxide [7631-86-9], SiO_2, of near-intrinsic purity. Other compositions could be produced as well using other chloride vapors such as phosphorus oxychloride [10025-87-3], $POCl_3$, and germanium tetrachloride [10038-98-9], $GeCl_4$, to dope the silica and provide changes in the refractive index of the glass. Two methods evolved. Inside vapor-phase deposition followed from chemical vapor deposition (CVD) processes used in the electronics industry (see ELECTRONIC MATERIALS; INTEGRATED CIRCUITS). When adapted for glass fabrication, chloride reactants were mixed with oxygen inside a silica tube which was externally heated. The chlorides were oxidized rather than hydrolyzed, producing particles of SiO_2 which adhered to the inner wall of the tube. The outside processes stemmed from the work in the 1930s (9) utilizing flame hydrolysis of SiO_2 to produce silica articles such as mirror blanks. Here $SiCl_4$ together with dopant precursors form a soot by passing the chlorides through a fuel−oxygen flame and depositing submicrometer-sized oxide particles on a mandrel.

3.2. Inside Processes.   *Modified Chemical Vapor Deposition.*   Inside processes such as modified chemical vapor deposition (MCVD) followed CVD techniques. In these the concentration of the reactants was kept low to inhibit homogeneous gas-phase reaction in favor of heterogeneous wall reactions which produce a vitreous (amorphous), particle-free deposit on the tube wall. Deposition was continued until a sufficient thickness of glass was produced; then the tube was collapsed to form a solid rod, or preform. This preform was then drawn to a relatively low loss fiber (10). Deposition rates by this method were impractically low, and attempts to increase them invariably led to the formation of particles and, subsequently, bubbles, resulting in excess scattering loss. The solution was to radically increase the reactant concentration and flow rates to more than 10 times those used for CVD. This led to the formation of SiO_2 and germanium oxide [1310-53-8], GeO_2, particles in the gas stream that were then deposited on the tube wall interior and fused by a traversing external torch. Multiple layers were deposited to achieve the desired refractive index profile before the tube was collapsed to a preform. The process was refined (11) to that depicted in Figure 5. First a high quality fused silica tube is mounted on a glass working lathe with a rotating joint for the injection of the reactants. High purity gases are then introduced into the rotating tube, which is traversed by an oxy−hydrogen torch. A homogeneous gas-phase reaction occurs in the hot zone created by the torch. The particles are small enough to be carried in the gas stream and deposited onto the tube walls downstream of the torch. As the torch passes, the particulate layer sinters to form a thin layer of highly pure oxide
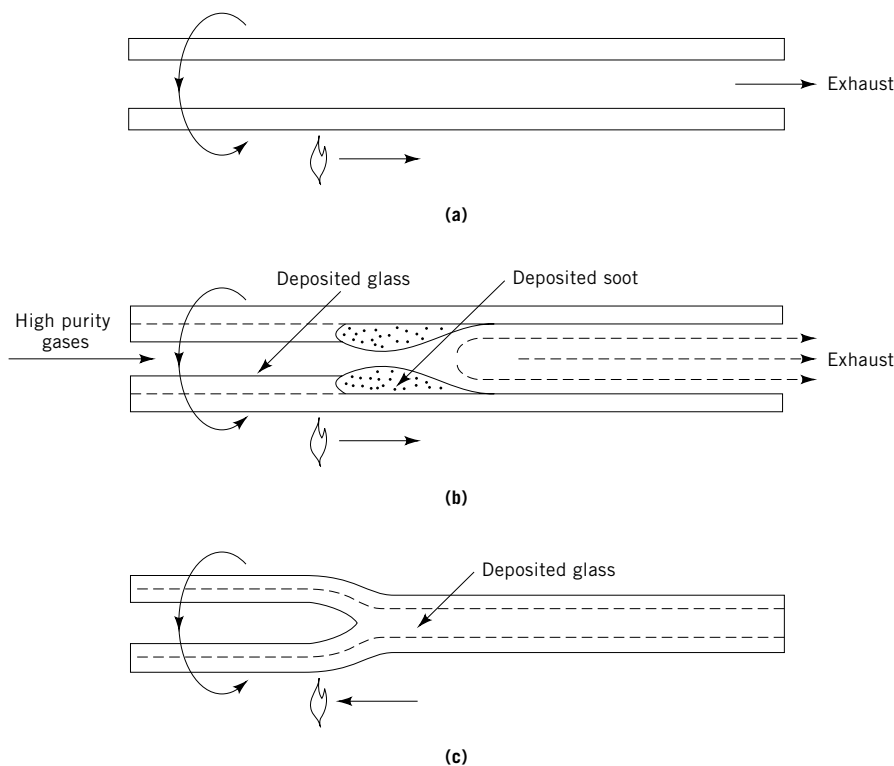
Fig. 5. Fiber formation by MCVD, where ⚡ represents the O_2-H_2 flame, showing (**a**), tube setup; (**b**), deposition; and (**c**), collapse.
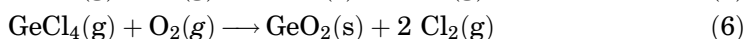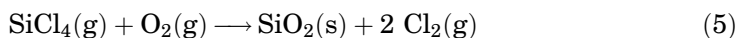
glass. The torch temperature must be kept high enough to fuse the glass layer without deformation of the substrate tube, as repeated deposition cycles are necessary to build up, layer by layer, the desired refractive index profile. The composition of each layer may be changed in order to manufacture highly complex structures. Typically 25 to 100 layers may be deposited to form either a graded-index multimode or single-mode optical fiber preform.

One of the areas critical to the MCVD process was understanding the chemistry of the oxidation reactions. It was necessary to control the incorporation of GeO_2 while minimizing OH^- formation. Additionally, understanding the mechanism of particle formation and deposition was critical to further scale-up of the process.

Thermophoretic Deposition. A fundamental understanding of how particles form and deposit on the tube walls was necessary for optimization of the deposition process. SiO_2 particles which form homogeneously in the gas phase have particle sizes of 0.02 to 0.1 μm and are carried in the gas stream. Without the imposition of a thermal gradient in the tube the particles remain in the gas stream and pass out of the tube; however, owing to temperature gradients caused by the traversing torch, thermophoresis occurs (12,13). Thermophoresis is a process by which particles in a temperature gradient travel toward the cooler region

when bombarded by more energetic particles on the hot side. In this case travel is outward from the center to the tube wall. Within the MCVD substrate tube the wall is only hotter than the gas in the hot zone of the torch where the oxidation reaction is occurring. Downstream the gas is hotter than the tube because of differences in thermal conductivity of the gas and silica, as well as to the flow of the gas. In the MCVD process (Fig. 5) the reactants enter the tube, are reacted in the hot zone of the torch, deposit thermophoretically downstream of the torch, and are subsequently sintered to a clear glass as the torch passes over the deposited particulate layer. Once the desired structure has been deposited, the direction of the torch is reversed and the tube is collapsed to form a solid preform.

Chemical Equilibria.   The chemistry of the MCVD process has been studied using a variety of techniques. Infrared (ir) spectroscopy (14,15) was used to investigate the oxidation reaction of $SiCl_4$ and $GeCl_4$ (see INFRARED TECHNOLOGY; RAMAN SPECTROSCOPY). The effluent gases from an MCVD reactor were fed into an infrared cell and analyzed to determine the reaction products as a function of temperature and composition. As the hot-zone temperature reached 1300 K, $SiCl_4$ began to react and form silicon oxychloride [14986-21-1], Si_2OCl_6. The partial pressure of silicon oxychloride increases to a maximum at 1450 K, above which concentrations of $SiCl_4$, Si_2OCl_6, and $POCl_3$ decrease until by 1750 K these concentrations become negligible in the effluent because all of the species have been converted to oxides. Germanium tetrachloride, $GeCl_4$, behaves some what differently. Up to 1500 K the pressure is constant; it then decreases until the reactor temperature reaches 1700 K, at which point it again stabilizes and grows slightly up to 2200 K. The majority of the initial species remains unreacted and is swept out of the reactor in the effluent. It was concluded from these results that at temperatures lower than 1600 K the degree of reaction of the $SiCl_4$, $GeCl_4$, and $POCl_3$ is controlled by reaction kinetics, whereas at higher temperatures the reaction is dominated by thermodynamic equilibria. Rate studies have shown that the residence times typically experienced in the hot zone are sufficient to reach equilibrium above 1700 K. The oxidation reactions for $SiCl_4$ and $GeCl_4$ are

$$SiCl_4(g) + O_2(g) \longrightarrow SiO_2(s) + 2\ Cl_2(g) \tag{5}$$
$$GeCl_4(g) + O_2(g) \longrightarrow GeO_2(s) + 2\ Cl_2(g) \tag{6}$$

The equilibrium constants for these reactions may be written as

$$K_{SiO_2} = \left(a_{SiO_2}\right)\left(P_{Cl_2}\right)^2 / \left(P_{SiCl_4}\right)\left(P_{O_2}\right) \tag{7}$$

and

$$K_{GeO_2} = \left(a_{GeO_2}\right)\left(P_{Cl_2}\right)^2 / \left(P_{GeCl_4}\right)\left(P_{O_2}\right) \tag{8}$$

where P_i are the partial pressures of the gaseous species, and a_i are the activities of the solid species. An approximation for the activities may be made using $\gamma_i \chi_i$, where χ_i are the mole coefficients. An activity coefficient of 1 implies ideal behavior, ie, obeying Raoult's law. The equilibrium constants for these reactions have

been determined as a function of temperature and it has been shown that equation 5 strongly favors the formation of SiO_2 at high temperature. The formation of GeO_2 according to equation 6 is repressed by Cl_2 formed from oxidation of $SiCl_4$ (eq. 5). The equilibrium constant for the $GeCl_4$ reaction approaches 1 above 1400 K. As a result only a portion of the $GeCl_4$ is converted to GeO_2. This fraction decreases with increasing temperature or chlorine partial pressure. Decreasing the partial pressure of oxygen shifts the germanium reaction even farther toward more unreacted $GeCl_4$.

Incorporation of OH is another critical aspect of the oxidation chemistry. Reduction to the ppb level is necessary for the manufacture of low loss optical fiber. Hydrogen is incorporated into the glass according to the reaction

$$H_2O + Cl_2 \longrightarrow 2\,HCl + \tfrac{1}{2}\,O_2 \tag{9}$$
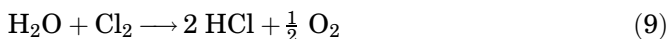
with the equilibrium constant

$$K_{OH} = \frac{(P_{HCl})^2 (P_{O_2})^{1/2}}{(P_{H_2O})(P_{Cl_2})} \tag{10}$$

The amount of OH incorporated into the glass, C_{OH}, is

$$C_{OH} = \frac{(P_{H_2O_{initial}})(P_{Cl_2})^{1/2}}{(P_{O_2})^{1/4}} \tag{11}$$

During the deposition phase of MCVD the chlorine level is between 3 and 10% owing to the oxidation of the chloride reactants. This level of chlorine leads to a reduction in the OH incorporation by a factor of about 4000. During the collapse phase of the process the chlorine level is significantly reduced and OH incorporation can be high as a result of the presence of hydrogen from either the oxy–hydrogen torch or impurities in the starting gases.

Sintering. The process by which the glass consolidates was found to be viscous sintering controlled by the viscosity of the glass at the consolidation temperature. The driving force is the reduction of surface energy via a decrease in the surface area. Because the soot layer is sintered by a moving torch, large thermal gradients may be present in the deposited layer ($\sim$300°C/cm). The time and temperature of consolidation must be controlled to allow a pore-free glass to result.

Plasma Chemical Vapor Deposition. Another process closely related to MCVD is plasma chemical vapor deposition (PCVD) (see PLASMA TECHNOLOGY) (16). This inside process uses the same precursor chemicals as MCVD to form a glass coating inside a tube which is collapsed to form a solid glass preform. The reaction within the tube, however, is quite different. Here the reaction is initiated by a nonisothermal microwave plasma which traverses the inside of the tube, as shown in Figure 6. The plasma requires a pressure of a few hundred Pascals and is generated by a microwave cavity which operates at 2.45 GHz. The glass is deposited not as a soot, but as a thin glass layer with efficiencies approaching 100%. In addition to the high efficiency, complex waveguide structures may be formed because many thin layers are produced by rapidly
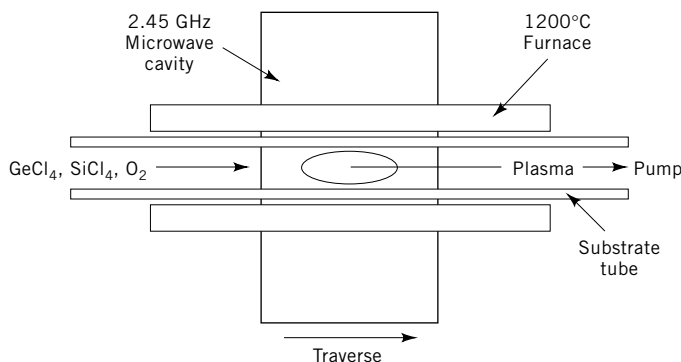
Fig. 6. Schematic diagram of PCVD deposition apparatus.

traversing the plasma. This method provides a smoother refractive index variation, which is especially advantageous for multimode fiber preforms.

3.3. Outside Processes. *Outside Vapor Deposition.* The outside vapor deposition (OVD) process developed by Corning Glass Works (17), is depicted in Figure 7. Soot is deposited layer by layer on a rotating mandrel at a temperature such that the soot particles are partially sintered. The precursor chemicals are the same as those used in the MCVD process but are oxidized by a gas−oxygen torch by similar chemical reactions. A doped core is deposited first followed by a SiO_2 cladding. The mandrel is removed and the porous preform consolidated at $1500-1600°C$ in a furnace with a controlled atmosphere containing helium, oxygen, and chlorine. The central hole may be collapsed either during sintering or fiber drawing, eliminating the need for a substrate tube. Additionally, dopants such as titania, TiO_2, may be added to the outer layers of the boule to improve fatigue resistance of the fiber drawn from it.

Vertical Axial Deposition. The vertical axial deposition (VAD) process (18) was developed by a consortium of Japanese cable manufacturers and Nippon Telephone and Telegraph (NTT). This process also forms a cylindrical soot form. However, deposition is achieved end-on without use of a mandrel and subsequent formation of a central hole. Both the core and cladding are deposited simultaneously using more than one torch. Whereas the OVD, PCVD, and MCVD processes build a refractive index profile layer by layer, the VAD process uses gaseous constituents in the flame to control the shape and temperature distribution across the face of the growing soot boule.

The design and engineering of the VAD torch, consisting of a series of concentric silica tubes, have been critical to its success. Reactants pass through the innermost rings. Shield gases separate these from oxygen and hydrogen in the outer rings, which form the flame. The soot plume and surface temperature of the boule are controlled by gas flows; temperatures and particle distributions in the flame are manipulated to provide the optimum surface temperature profile and tip shape.

Although the control in VAD is more difficult, this process has an advantage over OVD, especially for multimode fiber. The thermal mismatch between core and cladding materials caused by the heavy doping necessary to achieve the
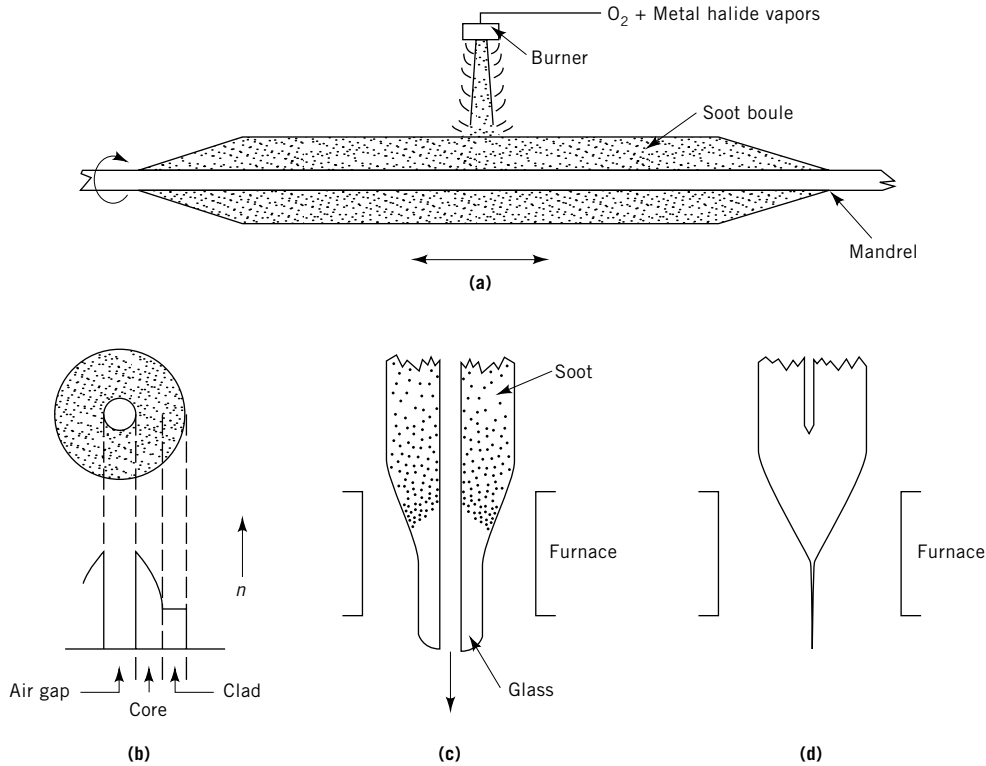
Fig. 7.   OVD process: (**a**) soot deposition, (**b**) soot perform cross section, (**c**) preform sintering, and (**d**) fiber drawing.

desired refractive index profile causes cracking in the OVD preforms at the inner surface as the glass cools through the glass transition, T_g. The VAD preforms withstand the stress because they possess no central hole to result in tensile stress. The primary obstacle for VAD was the creation of an optimized refractive index profile to minimize intermodal dispersion. Then it was discovered that the composition could be graded by control of the boule's surface-temperature distribution. This temperature distribution depends on the shape of the boule's growing face. Through understanding the relationship between the temperature and germania concentration (19), fiber properties equivalent to those formed by OVD and MCVD were achieved.

4. Fiber Drawing and Strength

Preforms manufactured by MCVD, PCVD, OVD, and VAD all must be drawn into fiber in a similar manner. Standard fibers are drawn to 125 μm in diameter from preforms on the order of 2 to 7.5 cm diameter. Fibers are drawn by holding the preform vertically and lowering it into a furnace. The preform is heated to a temperature at which the glass softens (2200°C) until a gob of glass stretches

from the tip of the preform and drops under the force of gravity. A neck-down region is formed at this point, providing the transition between preform and fiber. Fiber is drawn by means of a capstan system, and its diameter is controlled by a diameter monitor that adjusts the draw speed at a fixed furnace temperature. The result is long lengths of uniform fiber.

To preserve the intrinsic strength of the pristine glass surface, a polymer coating must be applied before the fiber is contacted by the capstan. The basic requirements for fiber drawing were known prior to the invention of low loss glass manufacturing techniques. However, stringent loss and strength requirements for optical fiber transmission systems necessitated optimization of the draw process. Figure 8 shows a fiber draw tower. Preforms are lowered by a feed mechanism into the furnace to keep the transition region at a constant temperature. The furnace may be a graphite resistance or a zirconia induction furnace, or any other clean heat source capable of achieving temperatures of 1950–2200°C. Graphite furnaces require the use of an inert gas shield to guard against oxidation of the heating elements. Zirconia furnaces must be maintained at a temperature greater than 1600°C owing to a large-volume change associated with a crystallographic transition in zirconia, which causes stress-induced fracture of the furnace tube. The advantage of the zirconia furnace is that an inert atmosphere is not necessary. Fiber diameter is controlled by a servo-system which controls the fiber draw speed using a monitor placed directly below the furnace. This device provides high (0.1-μm) resolution monitoring of the fiber diameter using a high update rate, eg, 500 Hz, which provides control to 0.29 μm (20). Such control is required for low loss fiber interconnection. Uniformity of the fiber diameter depends on the temperature control, preform feed rate, and pulling tension. Uniform preform diameters are required for low fiber diameter variability over long (>100 cm) distances whereas variations with a short period are caused by temperature fluctuations in the neck-down region. To control these perturbations the convective currents in the furnace may be controlled by appropriate baffling or controlled gas flow.

The strength of optical fiber is critical to its usefulness. Silica's intrinsic strength is very high (ca 14 GPa (2×10^6 psi)). However, in practice long lengths of fiber fail at considerably lower stress because of flaws which act as stress concentrators. The strength of the fiber is therefore determined by the largest flaw present in the length under test. Flaws may result from surface contamination, corrosion, and abrasion. In all cases cleanliness and care to avoid any physical contact with the unprotected fiber are required.

To protect the fiber surface a coating applicator is placed directly under the furnace as close as possible to the diameter monitor. The distance is controlled by the point at which the fiber temperature has dropped to 80°C (21). The fiber is coated upon passing through the cup containing a liquid polymeric coating and then passes through curing lamps or ovens before being taken up on a drum or spool. Typical coatings are uv-curable urethane acrylates and thermally cured silicone rubbers applied to a diameter of 250-μm (see RUBBER CHEMICALS; URETHANE POLYMERS). Beyond protecting the fiber from abrasion, coatings must be clean and free of particulate matter, concentric to the fiber, and have no voids. Low modulus coatings can improve the microbending performance of sensitive fibers by effectively cushioning the fiber. Dual coatings made up of a low [10^6–10^7 Pa
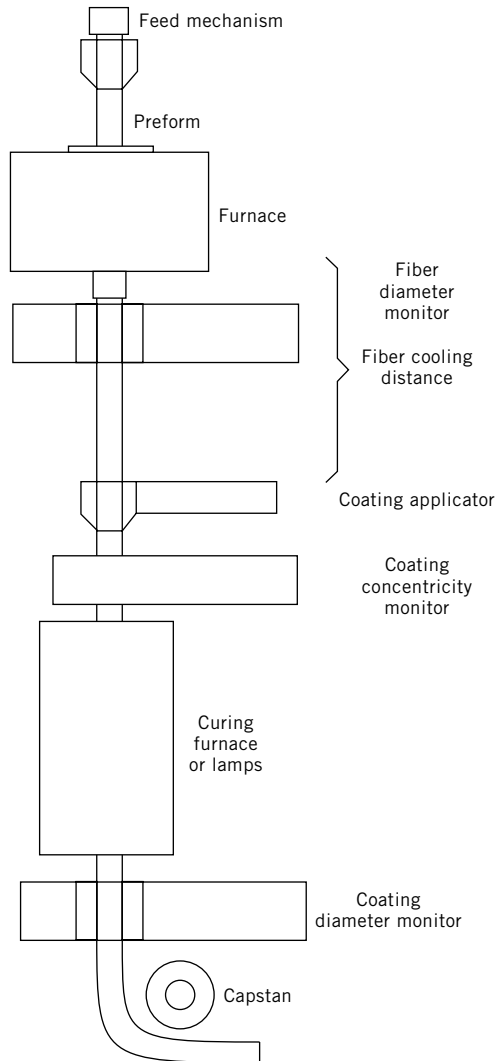
Fig. 8. Schematic of a fiber draw tower.

(150−1500 psi)] modulus elastomeric primary coating surrounded by a high modulus secondary coating are used for sensitive applications. Single coatings of high [10^9 Pa (150,000 psi)] modulus are used where strength is of primary concern.

An additional issue in fiber strength is that of fatigue (22), which can produce delayed failure of a fiber. Fatigue is thought to be caused by a surface reaction of fiber and OH causing the growth of subcritical flaws to the point where fracture occurs.

Although exact mechanisms have yet to be established, hermetic coatings (23) are being directly applied to keep contaminants from reaching the fiber surface. Polymeric coatings may be permeated by atmospheric moisture. A number of materials, metals and carbon, may be applied during the fiber drawing process, using vapor deposition. But only an amorphous carbon hermetic coating

has been commercialized. These coatings are primarily intended to protect the fiber from corrosion by water, but also prevent hydrogen-induced loss increases. Accelerated testing at high temperature or high H_2 pressure have been used to predict effects on the fiber over its lifetime.

The draw process itself, if not properly controlled, can lead to excess loss in the fiber. High draw tension (a combination of temperature and draw speed) can lead to losses associated with the breaking of Si–O bonds. High draw temperature may cause germanium suboxides to form which have well-defined absorption bands. Similar defects can be caused by the uv-curing lamps; however, short-uv filtering and uv-absorbing coatings can be used to ameliorate that problem (see COATINGS).

4.1. Overcladding.   Fiber manufacturing and drawing technology have advanced to the point that the optical losses are limited almost entirely by the intrinsic loss of the glass. Initially all of the fiber manufacturing processes (MCVD, PCVD, OVD, and VAD) produced preforms yielding on the order of 10 km of fiber. This situation changed as single-mode fiber usage grew. The proportion of core glass to the total amount of glass in single-mode fiber is much lower than in multimode fiber. Single-mode core diameter is ca 8 μm, multimode core diameter is 50 or 62.5 μm. This led to a desire for a method of manufacturing larger preforms by shrinking a second silica tube over the preform or depositing a thick soot layer on the preform to provide additional cladding. This procedure, known as overcladding, increased the length of fiber drawn from a single VAD preform to more than 100 km, for example, and significantly reduced the cost of producing fiber.

4.2. Sol–Gel Processing.   Fibers can be designed so that light only travels in the inner 30–40 μm of the fiber (24), which accounts for only about 5% of the fiber mass. Thus, using a core rod, the remaining 95% could be manufactured from less expensive, lower purity materials typically obtained by sol–gel processing (see SOL–GEL TECHNOLOGY). In the sol–gel technique silicon alkoxide [78-10-4], $Si_2(OC_2H_5)$, reacts with water in the presence of a catalyst and alcohol to form a sol. The sol can then be cast into a cylindrical mold where polycondensation of the silanol groups produces a siloxane gel network which eventually forms a semirigid gel. The gel body must then be dried and consolidated to form a glass. Alternatively, colloidal powders known as fumed silica can be formed into tubes by compaction (25), casting–gelation (26,27), and centrifugation (28). The mechanical compaction method uses dry silica which is packed into a mold, then consolidated at high temperature to form a glass. Centrifugation uses a cylindrical mold rotating at a speed of up to 35,000 rpm, forming a body which is subsequently dried and sintered. There are two methods for the casting–gelation technique. The first uses colloidal silica dispersed in an alkoxide sol. The sol acts as a binder during drying to prevent cracking. An alternative route uses fumed silica (colloidal) mixed with water and stabilized against agglomeration by the addition of surfactants (qv) (steric stabilization) or by control of the pH (electrostatic stabilization). The sol is then gelled (often by changing the pH), dried, and fired to a glass much as in OVD or VAD. During drying of gel bodies large stresses develop from shrinkage and capillary forces. These often cause the partially dried gel to fracture. Controlled drying is necessary for the formation of large gel bodies without cracking.

There has been a considerable effort to form all gel preforms from alkoxide gels using dopant elements such as germanium. Fibers produced using germanium ethoxide [14165-55-0], $Ge(OC_2H_5)_4$ (29), have not shown losses comparable to those made by vapor deposition techniques. A typical fiber produced by this technique contains included bubbles and an only slightly increased index in the core owing to germanium vaporization during firing (30). More success has been achieved in a silica-core-fluorine-doped cladding structure (31). The hydrolysis and polycondensation of monofluorosilicon ethoxide [358-60-1], $Si(OC_2H_5)_3F$, incorporates fluorine into the glass and this lowers the refractive index. This material is cast into a cylindrical body, gelled, and dried to form a porous tube having a surface area between 200 and 650 m^2/g. The high surface area makes it possible to consolidate the tube in a fluorine-containing atmosphere at low temperature, resulting in a down-doped tube having $\Delta = -0.62\%$. By collapsing this tube with a stream of oxygen flowing through the center, a core of higher index is formed as the oxygen removes fluorine from the inner surface of the tube. Losses of 0.4 dB/km have been reported.

For the production of large bodies the colloidal approach has yielded more success. These approaches are aimed at overcladding preforms produced by other methods.

4.3. Defects.   The ever-increasing demand for high data rate systems is forcing the search for an even greater understanding of those defects which produce attenuation of only hundredths of a dB/km. Profile control to produce zero dispersion at operating wavelengths is necessary, and environmental effects such as radiation and hydrogen exposure must be minimized. In addition, for reliability concerns, higher strength must be achieved with a narrow distribution, necessitating the understanding of flaw distributions and growth of flaws (fatigue).

5. Optical Amplifiers

Throughout the first two decades of their existence optical fibers served a passive role, ie, in the transmission of encoded light signals. In the late 1980s erbium-doped fiber amplifiers (EDFAs) were introduced (32,33), making it possible to amplify a 1.55 μm optical signal without first converting it to an electronic signal. The amplifier consists of a section (tens of meters) of single-mode optical fiber having about 100 ppm of erbium [7440-52-0] incorporated into the core. This fiber section becomes an amplifier when a continuous source of pump light, usually 0.98 or 1.48 μm, wavelength is propagating through the fiber. As the optical signal, usually 1.53 to 1.6 μm, travels through the length of fiber containing excited erbium ions, amplification occurs by the stimulated emission of photons from the excited state. Noise in the form of broad-band spontaneous emission accompanies this process; however, the signal-to-noise ratio is kept to an acceptable level even when cascading many of these devices for system applications. The device is shown in Figure 9.

A number of means have been developed to produce erbium-doped optical fibers. The task is complicated by the tendency of rare-earth ions to exsolve from high silica glasses. Rare-earth and alkaline-earth ions tend to compete
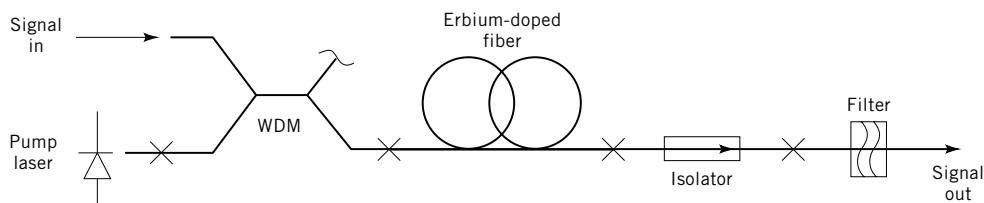
Fig. 9. Erbium-doped fiber amplifier where x represents splices and WDM is a wavelength division multiplexer combining the signal and pump wavelengths.

with silicon for oxygen ion coordination (see LANTHANIDES). Thus high silica glasses tend to phase-separate into two liquids at the high temperatures where fiber is drawn. Even rare-earth concentrations in the 100s of ppm undergo a subtle form of segregation. Association of these ions in the glass network (34) tends to cause interactions which lead to excited-state absorption. The situation is ameliorated by incorporation of homogenizer ions in the glass network. Aluminum is the most common of these. This trivalent ion can be thought to produce a charge deficiency which permits incorporation of erbium in adjacent sites.

The compatibility of aluminum and erbium extends to the vapor phase where complex aluminum—erbium chlorides exist at vapor-pressure orders of magnitude higher than $ErCl_3$. The passage of aluminum chloride, Al_2Cl_6, vapor over a heated erbium oxide, Er_2O_3, or erbium chloride, $ErCl_3$, source permit doping in MCVD reactions. In addition, erbium chelates and other organic precursors can be introduced into VAD or OVD flows to produce doped soot. Finally, doping with solutions containing rare-earth ions or sol–gel doping of soot or MCVD substrate tubes prior to the final collapse to a solid preform also provide the means for controlled introduction of the ions.

EDFAs are being introduced into long-distance, particularly undersea, systems which operate at wavelengths near 1.6 μm. In addition to providing an inexpensive means of amplification EDFA also make it possible to amplify numerous wavelengths near 1.6 μm, whereas semiconductor amplifiers suffer crosstalk when amplifying more than one wavelength (see SEMICONDUCTORS).

6. Fiber Optic Sensors for Smart Structures

6.1. General.   Man-made structures can be made "smart" by duplicating the essential elements of the system that consists of embedded sensors, data links, a programmed data processor, and actuators. Fiber-optic sensors offer embedded sensor capability and natural connections to fiber-optic data links that can be used in a wide variety of composite materials to act as the structure's "nervous system." These sensors have a series of important advantages over conventional electronic sensors. (*1*) They are small and often made in overall diameters of 125 microns or less that results in a hair thin sensor that can be embedded in many types of composite structures without changing mechanical properties. (*2*) Fiber-optic sensors can be made environmentally rugged and can withstand the temperatures and pressures in manufacturing composite

structures. (*3*) The glass fibers are passive dielectric devices that enable their usage in organic composite materials like carbon epoxy and thermoplastics where electrical discharge hazards such as lightning on aircraft and spacecraft require eliminating conductive paths. The passive nature of fiber-optic sensors also allows embedding these sensors successfully into metal structures. (*4*) Many fiber-optic sensors can be made that have a high degree of immunity to electromagnetic interference and eliminate the need for costly and bulky shielding. (*5*) Fiber-optic sensors may be multiplexed, so that many sensors lie along a single fiber line. (*6*) Fiber sensors are naturally compatible with fiber-optic data links that have the bandwidth necessary to support large number of sensors. (*7*) There is a high degree of synergy between fiber-optic sensors and the telecommunication and optoelectronics industry that leads to continuously improve components and lower costs.

6.2. Theory. A basic block diagram of a fiber-optic smart structure system is shown in Figure 10. A composite panel may have embedded or attached fiber-optic sensors that are used to monitor an environmental effect. These sensors may be multiplexed, and their signals are carried by a fiber-optic data line to an optical/electronic processor which is used to sort and preprocess the information. Then, the data are formatted and transmitted to a control system that may be used to support performance enhancement or act to assess damage. A fiber-optic link may then be used to convey information to an actuator system that is directed to respond to the environmental effect.

There are many issues in implementing this type of system, including placement of the fiber in the composite material (36−38) without degrading the strength of the structure, the coating on the fiber (39−42) which is crucial to successful sensing, ingress and egress out of parts (43−45), what type of fiber sensors to use, and what type of multiplexing (46−50) and signal processing (51−55). Overriding all of these issues are the concerns of the end user and system designer (56−58) who passes down requirements that must be met by all of these subsystems.
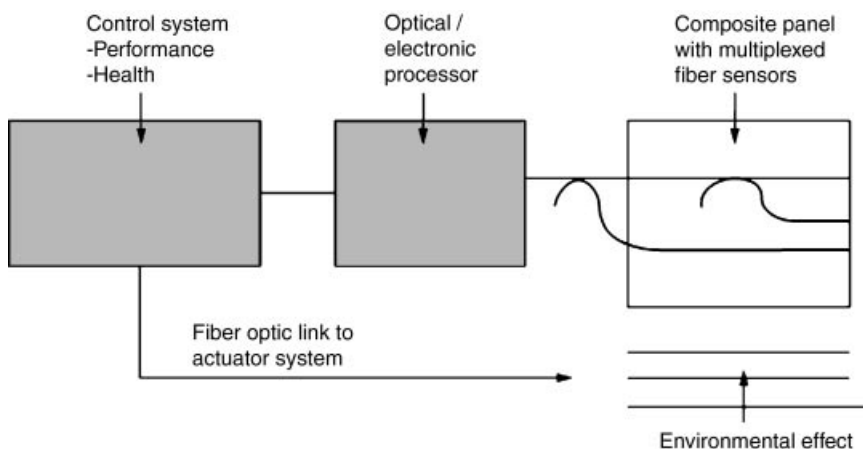

Fig. 10. Fiber-optic smart structure system. Reprinted with permission from Ref. 35.
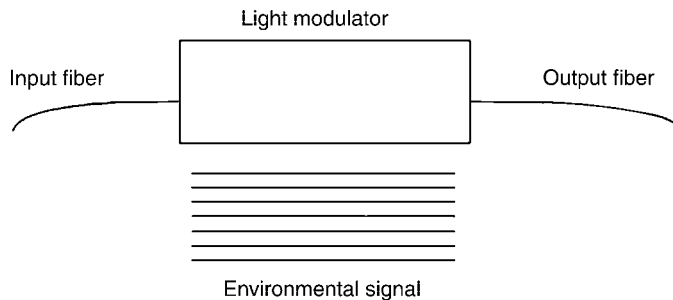
Fig. 11.   Extrinsic fiber-optic sensors. Reprinted with permission from Ref. 35.

Two types of fiber sensors are commonly used. The first, called extrinsic or hybrid fiber optic sensors and illustrated by Figure 11, consists of an optical fiber leading up to and away from a "black box." Environmental information is impressed onto the light carried by the optical fiber through the action of this "black box" that may be in the form of amplitude, phase, polarization, or other types of modulation of the light beam. The second type of fiber optic sensor shown in Figure 12 is called the intrinsic or all fiber sensor. Here, the light beam is modulated in the fiber by an environmental effect.

Because of concerns about the structural degradation of composite materials, it is often desirable to have a fiber sensor whose overall diameter is not much larger than a standard, 125-micron telecommunication grade optical fiber. This often does not apply to large concrete structures and instead is usually used for relatively thin composite structures. Figure 13 shows an example of a microbend-based fiber sensor. Here, a light source couples light into an optical fiber, and an environmental effect acting on a microbend transducer modulates the light intensity passing through the fiber. The greater the localized bending, the higher
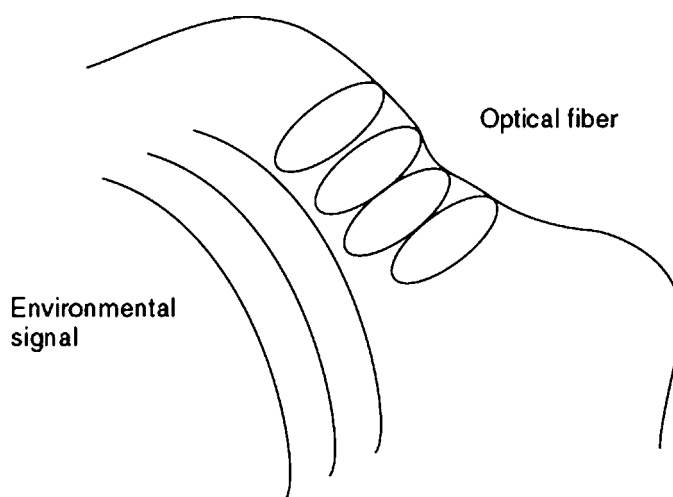

Fig. 12.   Intrinsic fiber-optic sensors. Reprinted with permission from Ref. 35.
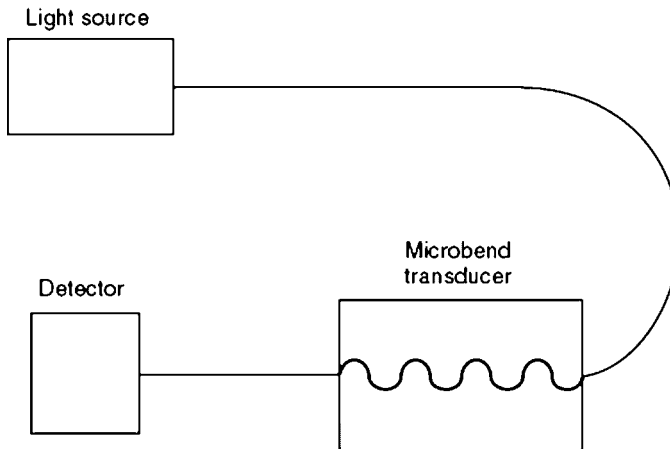
Fig. 13. Microbend fiber sensors. Reprinted with permission from Ref. 35.

the loss. In composite materials, this can be realized by placing the optical fiber orthogonal to the strength members of the composite or by using specially designed jackets that optimize microbend sensitivity (59).

The microbend sensor has the advantage that it is very simple and is usable when high accuracy is not required. For higher precision applications, problems arise that include variable loss in connectors, macrobending loss, incidental microbending loss, and mechanical misalignment. Each of these effects could cause intensity changes that might be misinterpreted as arising from an environmental effect to be measured. One way to overcome these limitations is to adopt spectrally based approaches. For intensity-based fiber sensors, this often means using two separate wavelengths where one wavelength measures intensity losses throughout the system and the other measures intensity losses everywhere except in the sensing region. By differencing these signals, the environmental effect may be more accurately measured. Another approach is to use a fiber-optic sensor that is inherently spectral. These sensors may be based on blackbody radiation, absorption, fluorescence, dispersive elements such as gratings, and etalons or other spectrally sensitive elements.

Figure 14 is a diagram of a blackbody temperature sensor. When the blackbody cavity at the end of the fiber is heated, it changes temperature and emits radiation. The light is then gathered by the optical fiber and spectrally analyzed
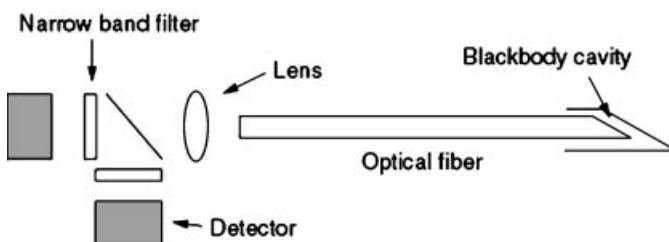

Fig. 14. Blackbody sensor. Reprinted with permission from Ref. 35.
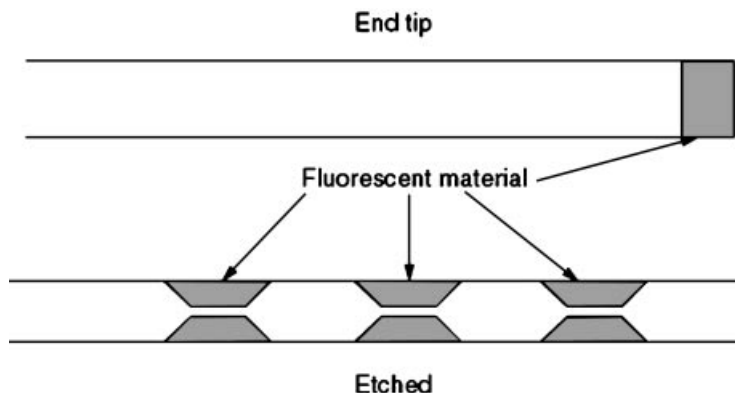
End tip

Fluorescent material

Etched

Fig. 15.   Fluorescent probes. Reprinted with permission from Ref. 35.

by placing narrowband optical filters in front of detectors. As the blackbody cavity heats up, the curve shifts to the shorter wavelengths associated with higher temperatures. By taking samples of the spectrum at points on these curves, the spectral envelope may be defined, and the temperature is extracted.

Another type of spectral sensor that can be used for a wide variety of parameters, including temperature, pressure, viscosity, and chemical content is a fiber sensor based on a fluorescent (or absorptive) probe, as shown in Fig. 15. In the end tip configuration, the light beam propagates down the optical fiber and encounters a fluorescent material plug. The material fluorescence depends upon a physical effect such as temperature or pressure and can also be influenced by the presence or absence of chemical species. Different modes of operation are possible. The relevant parameter for a pulsed light source could be the rate of decay of the fluorescence. The parameter of interest for a continuously operated light source could be the spectral content of the fluorescing signal. Another configuration of the fluorescent probe is made by etching away some of the glass cladding and replacing it by fluorescing material. The evanescent field of the light beam is then used to stimulate these areas. By separating these regions physically and using a short light pulse in combination with materials that have a fast rate of fluorescent decay, time division multiplexing techniques may be used to support multiple sensors.

The key parameter of interest for many types of structures is often strain. Because much of traditional structural analysis and experiment have been supported by strain sensors of relatively short gauge length and many events occur over relatively short distances, a fiber optic strain sensor of short gauge length is highly desirable. Fiber gratings and fiber etalon-based fiber-optic sensors meet these requirements.

A fiber grating (60–63) may be formed by exposing the core of a germanium-doped optical fiber to alternating regions of highly intense and dark short wavelength laser light. This may be done by using a phase mask and a high intensity uv light source or, as in Figure 16, by combining two laser beams to form an interference pattern that is imaged through the side of the fiber that "writes" the grating pattern onto the fiber. The major issue for the fiber grating is that
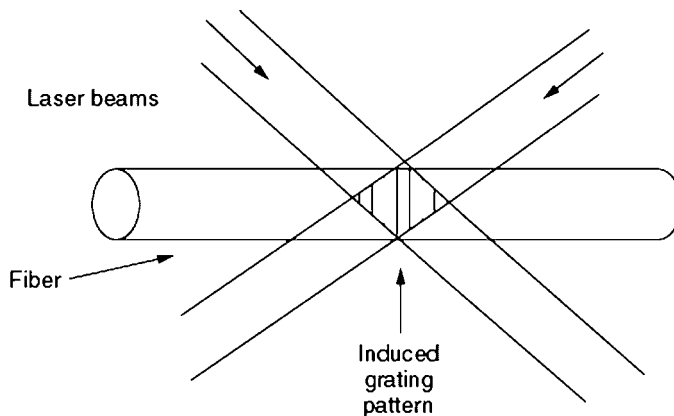
Fig. 16. Fiber grating. Reprinted with permission from Ref. 35.

the change in wavelength for small strains of the order of 10 microstrains can be quite small, on the order of 10^{-2} nm, because this is below the resolution level of most laboratory spectrometers that are too expensive to be cost-effective, the major issue has been to find methods that can be used to extract the strain information. This can be done by a number of methods. Essentially what is needed is a narrowband spectral filter to beat against the spectral profile of the fiber grating. This filter can be as simple as a second fiber grating that is matched to the first. Then, the reference fiber grating can be modulated and adjusted in length to match the fiber grating used to sense strain in the composite material. Other approaches include using filters based on Fabry–Perot etalons and interferometers.

Various types of Fabry–Perot etalons (64–71) are shown in Figure 17. In each example, light transmitted through the etalon, which consists of two reflective surfaces, is transmitted at the highest efficiency when the wavelength of the light is such that an integral number of waves at that wavelength corresponds to the distance between the two mirrors. The sharpness of transmission peak will vary, depending on the reflectivity of the mirrors. Higher values of finesse represent higher mirror reflectivities. The two most common ways to make a fiber etalon are shown in Fig. 10. The intrinsic fiber etalon consists of fibers that have been cleaved and coated by a reflective material. This could be a metal or a dielectric material such as titanium dioxide. The fibers are then refused to form a mirror contained within the fiber. The process is repeated twice to form an intrinsic fiber etalon. A second approach is to take a capillary tube and insert reflectively coated (or bare) fibers into it. The first approach has the advantage that is no larger than the fiber diameter that has an issue of polarization control. The second approach eliminates the polarization problem at the cost of overall size and ruggedness. A third configuration uses two fibers reflectively coated and placed in close proximity to form a variable etalon (spectral filter) that can be used to demodulate fiber gratings.

There are some applications where fiber optic strain sensors of long gauge length are useful, including monitoring earth movement and strain on high tension wires. Here, interferometeric fiber sensors can be extremely useful.
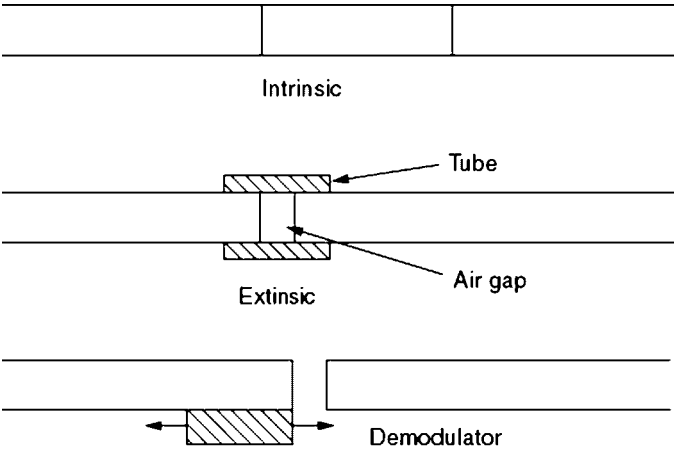
Fig. 17.   Fiber etalons. Reprinted with permission from Ref. 35.

Figure 18 shows a block diagram of a Sagnac interferometer configured to measure slowly varying events such as strain (72). A light source and beam conditioning optics are used to generate counterpropagating light beams about a fiber coil. A frequency shifter is placed in the coil to generate a frequency difference between the counterpropagating light beams in the loop. If the loop is changed in length by an amount dL, the frequency difference F is changed between the counterpropagating beams to keep the relative phase of the beams constant, then $dF/F = -dL/L$, and the change in frequency can be used to measure the change in length.

Another class of fiber-optic sensor that has the potential for wide use in fiber-optic smart structures is the distributed fiber sensor (73–76). Most of these sensors are based on variants of optical time domain reflectometry and look at forward or backward scatter of light beams. Scattering mechanisms that have been used include Rayleigh, Raman, Brillouin, and fluorescence. A few have been based on nonlinear effects such as the Kerr effect. Figure 19 shows a distributed fiber sensor based on Rayleigh backscatter that uses a
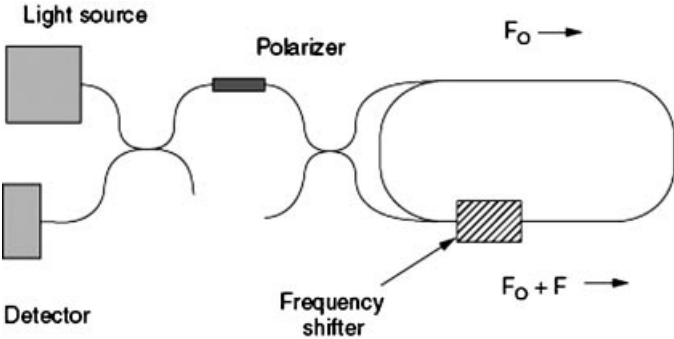

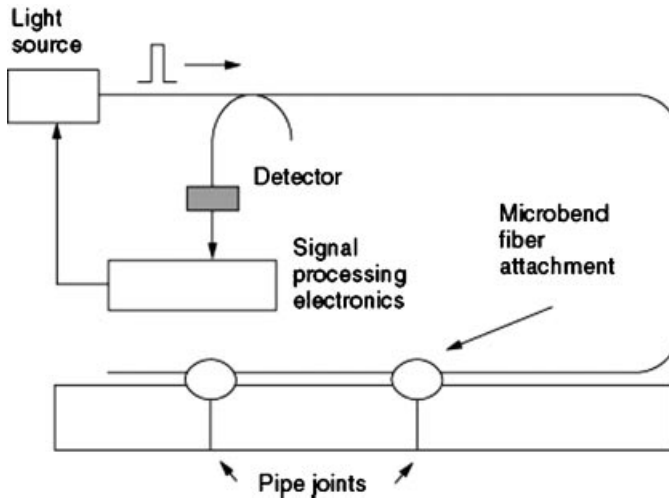**Fig. 18.**   Quasi-static sensing-strain. Reprinted with permission from Ref. 35.

Fig. 19. Distributed sensors based on Rayleigh scattering. Reprinted with permission from Ref. 35.

microbend-sensitive fiber attached to strain points on a pipeline. The excess scatter and loss at these points is used as an indication of strain. Raman scattering has been used effectively to measure temperature along the length of the fiber because this type of scattering has strong temperature dependence. Distributed fiber sensors may also be used to locate and measure time-varying effects such as acoustic or vibrational disturbances. Interlaced Interferometeric fiber sensors can do this. They are all based on the position-dependent response of the Sagnac interferometer and include combinations of the Mach–Zehnder and Sagnac interferometer as well as multiple Sagnac configurations. Figure 20 illustrates a wavelength division multiplexed Sagnac distributed sensor. The key point is that if a time-varying disturbance occurs in the center of the Sagnac loop, the net phase difference between the two counterpropagating beams is zero because both beams arrive at this point simultaneously. As the disturbance moves along
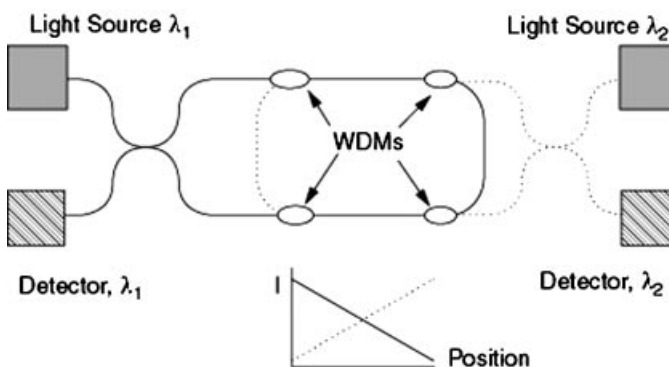

Fig. 20. Interlaced Sagnac loops. Reprinted with permission from Ref. 35.

the loop back to the coupler that originated the counterpropagating beams, the signal level for a fixed frequency scales up linearly, as the time difference between the arrival of the counterpropagating light beams increases. By interleaving two Sagnac interferometers at two different operational wavelengths, two linear responses are generated to a time-varying effect whose sum is a measure of the amplitude of the effect and whose ratio indicates position.

6.3. Applications.   Most fiber-optic smart structure applications (72–85) fall into one of four major categories. The first is smart manufacturing where fiber-optic sensors are embedded or attached to parts during the manufacturing process. They are then used to monitor such parameters as temperature, pressure, viscosity, degree of cure, and residual strain. After the parts have been made, the same sensors or another set may be used for the second application area of nondestructive testing. Here, the fiber sensors may be used to measure acoustic signatures, changes in strain profiles, delamination, and other indications of changes in the structural characteristics of fabricated parts. The third aspect of fiber-optic smart structures that has been the focus of many efforts is health and damage assessment systems for structures. In the parts of the structure that have been assembled, fiber-optic sensor technology is used to monitor the overall health of the structure. Examples include the status of buildings, bridges, and dams and checks to support the maintenance of aircraft. Finally, fiber-optic smart structures may be used to support control systems. Unlike health and damage assessment systems, which simply monitor changes in the structure, these control systems measure the environmental effects that act on the structure and then react to them. Examples of these types of structures are buildings that sense and readjust to earthquakes to minimize damage and airplanes that are designed to react to structural changes by adjusting their flight envelopes.

One potentially very large application area for fiber-optic smart structures is smart manufacturing. Figure 21 illustrates the concept of embedding an optical fiber in a composite part that is being processed in an autoclave. The embedded fiber may be used to measure temperature and degree of cure based
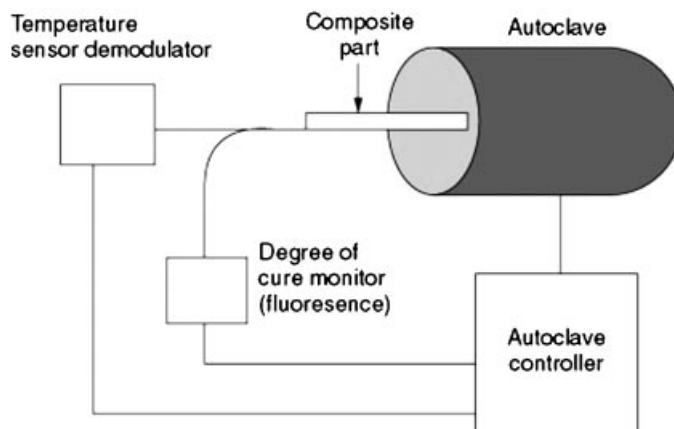

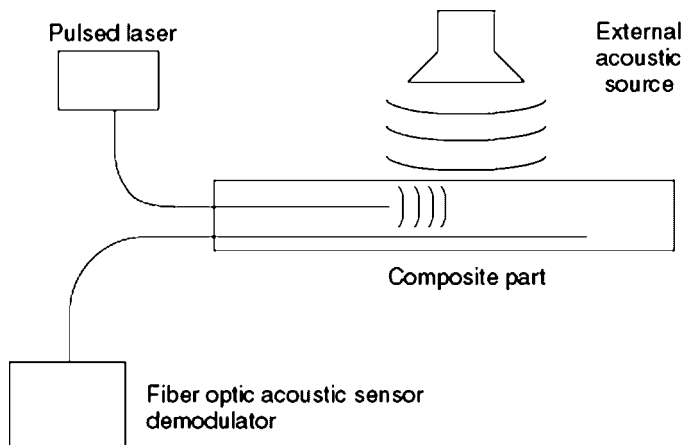**Fig. 21.**   Smart manufacturing. Reprinted with permission from Ref. 35.

Fig. 22. Nondestructive evaluation. Reprinted with permission from Ref. 35.

on the fluorescence of the resin in the composite part. Because large composite parts are often very high value items, it would be highly desirable to improve the reliability of part processing. Variations in resins from batch to batch and those due to aging can change optimum processing parameters. Internal measurements of key parameters offer the prospect of improving this situation. The key obstacles to widespread usage are that manufacturing personnel are not familiar with fiber-optic sensors, there are logistical difficulties in connecting the fibers to the parts, and effective low-cost fiber sensors are not available. This is slowly changing as more personnel are trained to use fiber optics, as components, and methods improve, and as higher production rates are achieved for key components.

A similar situation applies to nondestructive testing of parts (86,87). Figure 22, shows how acoustic sources are used to perform diagnostics on parts after fabrication. Fiber-optic acoustic sensors are buried internally in the part and can be used for local measurements. Other types of fiber-optic sensors could be used to support nondestructive testing and could be the same ones used to support smart manufacturing.

One of the most widely investigated system applications is damage assessment (72–83). Many of these systems use strain or acoustic sensors to monitor changes caused by impact on a structure. Figure 23 illustrates a system that consists of a thermoplastic panel in which a 3×3 array of microbend-sensitive optical fibers has been embedded. Light sources and detectors are placed to monitor intensity level changes in light that propagates through the fibers. When a steel ball is dropped on the panel, there is a characteristic signal that can be recognized by a neural network, and the force of the impact is determined. Because many composite materials are locally asymmetrical, the signal that reaches a particular sensor from the right or left may also have a different characteristic signature that enables the neural network to determine whether an event occurred to the right or the left of a sensor. This information can in turn be used to determine the location and the force and damage of an impact.
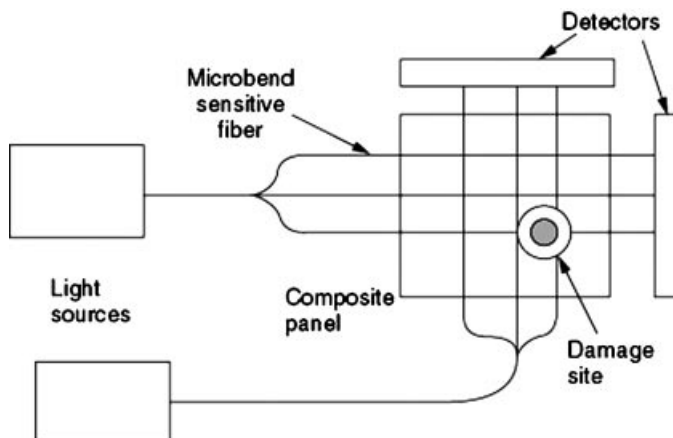
Fig. 23.   Damage assessment. Reprinted with permission from Ref. 35.

Implementing a damage or control system on a large structure such as an aircraft wing can require large numbers of sensors. As an example, measuring strain fields across the entire wing of a large modern jetliner (an MD-11, 767, or 777) would require about 2000 sensors based on placing fiber strain sensors approximately every 10 cm. To make a system affordable, it generally must be a small fraction of the total structural cost and most importantly, it must create substantial economic value for the end user. This value added could be improved safety, reliability, or maintainability. It could also be measured in terms of fuel savings for an aircraft or customer downtime for utility applications. Whatever measures and justifications are used, they must be clear for a viable commercial application to occur. Several possible architectures are possible for realizing such a system. One approach is to use fiber-optic sensors that have wide area coverage to locate damage approximately and then switch to a more comprehensive set of sensors for a detailed assessment later. A second approach is to configure a large number of fiber-optic sensors for detailed sensing but have only a small fraction on in a quiescent state for an initial localization of damage.

Figure 24 shows a module that could be used to support a system that has a large number of sensors. Strings of fiber sensors that could be fiber gratings or fiber etalons are multiplexed along a single fiber line. Several of these strings are connected to an optical switch that may be used in conjunction with a demodulator unit to interrogate subsets of the fiber sensors on the string. By switching between strings and measuring the output of selected sensors along the selected string(s), localized detailed assessments may be made without overwhelming processor capabilities to form real or nearly real-time measurements. The information from the demodulator is then formatted for transmission via a fiber-optic data link to a subsystem signal processor that could be used to support many modules consisting of formatter/demodulator/switch units. The information from the subsystem signal processor would then be routed to a health management bus. For an aircraft, this would be a vehicle health management bus that
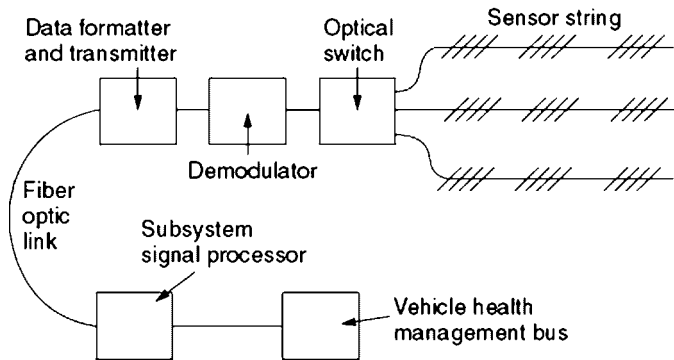
Fig. 24. Modular architecture. Reprinted with permission from Ref. 35.

has an avionics architecture similar to that of Fig. 25. The damage assessment information on the bus would be processed and routed via distribution systems to the pilot or automatic systems that would react and take necessary corrective actions.

Building and bridges (88–90) could have similar systems to monitor for earthquake damage, fires, break-ins, and other events that require corrective action. The information could be routed via communication links (that might also be fiber-optic based) to a central monitoring station, as in Fig. 26. As cable TV and telephone services improve, it can be expected that these sensing systems will form a natural extension of existing services.

Fiber-optic smart structures also may be used to provide new capabilities for monitoring very large natural structures (91). One exciting possibility is the use of very long fiber-optic strain sensors in combination with existing
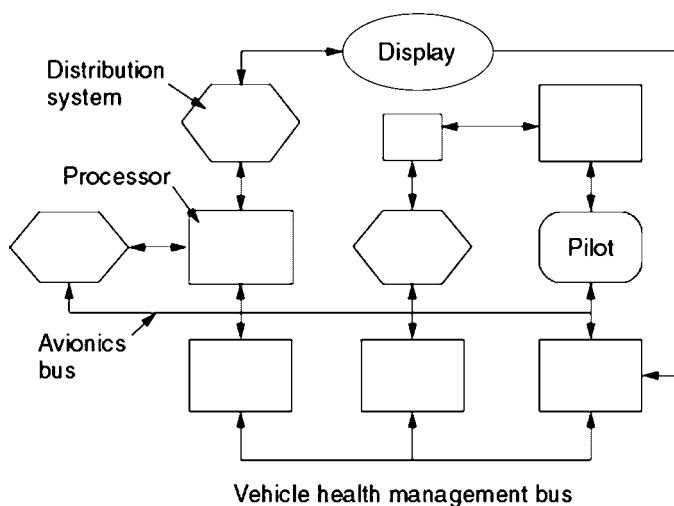

Fig. 25. Avionics example. Reprinted with permission from Ref. 35.
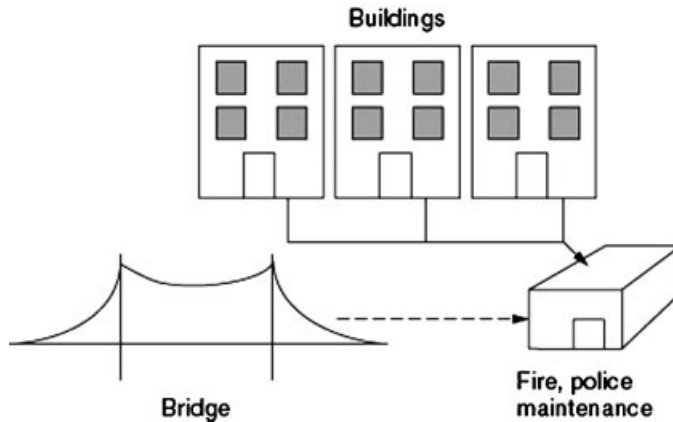
Fig. 26. Fiber-optic civil structures. Reprinted with permission from Ref. 35.

fiber-optic telecommunication links to provide a wide base of information on strain buildup near fault areas. This information could be used to form a database that may provide a future basis for earthquake prediction and more rapid monitoring of events. Figure 27 illustrates how this type of system could be locally configured. Fiber-optic communication cables pass near a fault line. Fiber-optic sensors (such as the Sagnac strain sensor of Fig. 18) are used to measure small changes in strain parallel to the fault line. This information is then converted into digital form and transmitted back to a central processing location. Monitoring fault lines in California or Japan would be examples of the way this system could be deployed. Other examples could be monitoring earth movements by measuring strain buildup in volcanoes.

There are also cases where earth movements that result in rock slides or displacement of buildings or other high value assets are important to measure. Figure 28 shows an oil drilling platform that may be slowly moved by currents or river outflow. Fiber-optic strain systems could be part of a smart structure
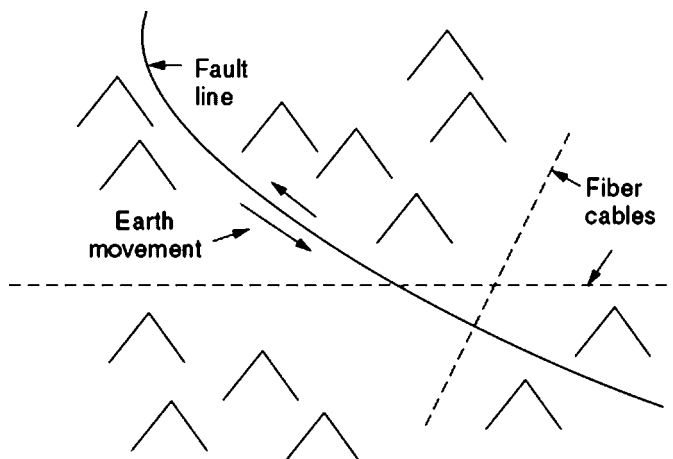

Fig. 27. Earth movement detection system. Reprinted with permission from Ref. 92.
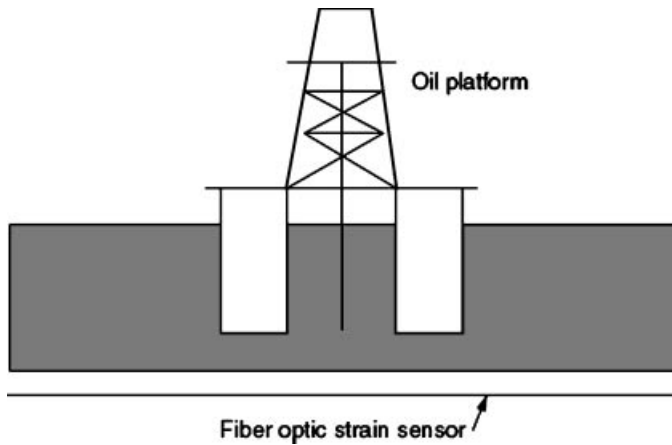
Fig. 28.   Monitoring oil platform motion. Reprinted with permission from Ref. 92.
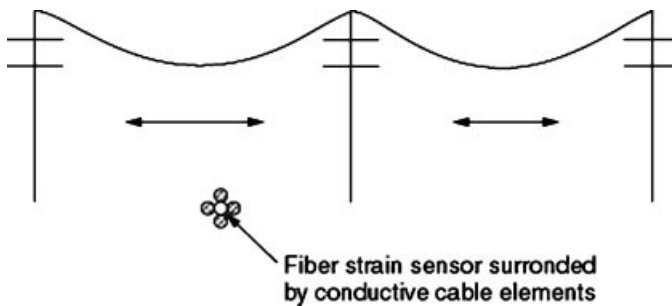

Fig. 29.   Stress on power lines. Reprinted with permission from Ref. 92.

system to monitor the position and strain buildup on the platform. Another example in Fig. 29 shows how fiber-optic strain sensors of long gauge length could be placed in power or telecommunication cables. Strain buildup could then be monitored for ice storms or earth slippage.

7. Acknowledgment

BIBLIOGRAPHY

"Fiber Optics" in *ECT* 3rd ed., Vol. 10, pp. 125–147, by A. D. Pearson and J. D. MacChesney, Bell Laboratories, Inc., and W. G. French, 3M Co.; in *ECT* 4th ed., Vol. 10, pp. 514–538, by Sandra Kosinski and J. B. MacChesney, AT&T Bell Laboratories;

"Fiber Optics" in *ECT* (online), posting date: December 4, 2000, by Sandra Kosinski and John B. MacChesney, AT&T Bell Laboratories.

CITED PUBLICATIONS

1. S. Miller, *Sci. Am.* **214**, 19–27 (1966).
2. S. E. Miller and L. C. Tillotson, *Appl. Opt.* **5**(5), 1538–1548 (1966).
3. P. Kaiser, *Bell Syst. Tech. J.* **49**, 137–153 (1970).
4. E. A. J. Marcatili and R. A. Schmeltzer, *Bell Syst. Tech. J.* **43**, 1783–1809 (1964).
5. H. Hosono, Y. Abe, D. L. Kinser, R. A. Weeks, and H. Kawazoe, *Phys. Rev. B.* **46**, 1144–11451 (1992).
6. L. G. Cohen "Ultrabroadband Single-Made Fiber", Paper No. MF4 in the *Technical Digest of Fiber Communications Converence, New Orleans, La.*, Optical Society of America, Washington, D.C., 1983.
7. A. D. Pearson and W. G. French *Bell Labs. Rec.* **50**, 103–106 (1972).
8. K. J. Beals and C. R. Day, *Phys. Chem. Glasses* **21**, 5–19 (1980).
9. U.S. Pat. 2,272,342 (Aug. 27, 1934), J. F. Hyde (to Corning Glass Works).
10. J. B. MacChesney and co-workers, *Phys. Lett.* **23**, 340–341 (1973).
11. J. B. MacChesney, P. B. O'Connor, F. V. DiMarcello, J. R. Simpson, and P. D. Lazay, "Preparation of Low-Loss Optical Fibers Using Simultaneous Vapor-Phase Deposition and Fusion," in *Proceedings of the Tenth International Congress on Glass, Kyoto, Japan*, Vol. 6, Ceramics Society, Japan, 1974, pp. 50–54.
12. P. G. Simpkins, S. G. Kosinski, and J. B. MacChesney, *J. Appl. Phys.* **50**, 5676–5681 (1979).
13. K. L. Walker, F. T. Geyling, and S. R. Nagel, *J. Am. Ceram. Soc.* **63**, 96–102 (1980).
14. D. L. Wood, K. L. Walker, J. B. MacChesney, J. R. Simpson, and R. Csencits, *J. Lightwave Technol.* **LT-5**, 277–283 (1987).
15. K. L. Walker, J. W. Harvey, F. T. Geyling, and S. R. Nagel, *J. Am. Ceram. Soc.* **63**, 92–96 (1980); S. G. Kosinski, L. Soto, and S. R. Nagel, "Characterization of Germanium Phosphosilicate Films Prepared by MCVD," presentation, at the fall meeting of the American Ceramic Society, 1981, Bedford, Pa., 1981.
16. D. Kuppers and H. Lydtin, *Preparation of Optical Waveguides with the Aid of Plasma-Activated Chemical Vapor Deposition at Low Pressures in Topics in Current Chemistry*, Vol. 89, Springer-Verlag, Berlin, 1980, pp. 108–130.
17. U.S. Pat. 3,737,292 (1973), D. B. Keck, P. C. Schultz, and F. Zimar.
18. T. Izawa and N. Inagaki, *Proc. IEEE* **68**(10), 1184–1187 (1980).
19. T. Edahiro, M. Kawachi, S. Sudo, and S. Tomaru, *Jpn. J. Appl. Phys.* **19**, 2047–2054 (1980).
20. D. H. Smithgall and R. E. Frazee, *Bell Syst. Tech. J.* **60**, 2065 (1981).
21. V. C. Paek and C. M. Schroeder, *Appl. Opt.* **20**(7), 1230–1233 (1981).
22. C. R. Kurkjian, J. T. Krause, and M. J. Matthewson, *J. Lightwave Technol.* **7**(9), 1360–1370 (1989).
23. R. G. Huff, F. V. DiMarcello, and A. G. Hart, Jr., "Amorphous Carbon Hermetic Optical Fiber," paper no. TuG-2 in *Technical Digest of Optical Fiber Communications Conference, New Orleans, La.*, Optical Society of America, Washington, D.C., 1988.
24. J. B. MacChesney, D. W. Johnson, P. J. Lemaire, L. G. Cohen, and E. M. Rabinovich, "Fluorosilicate Substrate Tubes to Eliminate Leaky-Mode Losses in MCVD Single-Mode Fibers with Depressed Index Cladding," paper no. WH2 in *Technical Digest of Optical Fiber Communications Conference, San Diego, Calif.*, Optical Society of America, Washington, D.C., 1985.

25. R. Dorn and co-workers, *Glastech. Ber.* **66**, 29–32 (1987).

26. P. Bachmann, P. Geitner, H. Hydton, G. Ronanowski, and M. Thelen, "Preparation of Quartz Tubes by Centrifugal Deposition of Silica Particles," in *Proceedings of the 14th European Conference on Optical Communications, Brighton, UK*, IEE, London, 1988, 449–453.

27. T. Mori and co-workers, *J. Non-Cryst. Solids* **100**, 523–525 (1988).

28. N. Okazaki, T. Kitagawa, S. Shibata, and T. Kimura, *J. Non-Cryst. Solids* **116**, 87–92 (1990).

29. S. Shibata and T. Kitagawa, J. *J. Appl. Phys.* **25**, L323–L324 (1986).

30. K. Susa, I. Matsuyama, S. Satoh, and T. Suganuma, *J. Non-Cryst. Solids* **119**, 21–28 (1990).

31. S. Shibata, T. Kitagawa, and M. Horiguchi, "Wholly Synthesized Fluorine-Doped Silica Optical Fiber by the Sol-Gel Method," in *Technical Digest of the 13th European Conference on Optical Communication, Helsinki, Finland*, Association of Electrical Engineers of Finland, Helsinki, 1987, 147–150.

32. E. Desurvire, J. R. Simpson, and P. C. Becker, *Optics Lett.* **12**, 888–890 (1987).

33. R. J. Mears, L. Reekie, I. M. Jauncey, and D. N. Payne, *Electron. Lett.* **23**(19), 1026–1028 (1987).

34. U.S. Pat. 466,624 (1987), J. B. MacChesney and J. R. Simpson (to AT&T).

35. E. Udd, *Fiber Optics Sensor Workbook*, Blue Road Research, Fairwood, Or, 1993.

36. R. L. Wood, A. K. Tay, and D. A. Wilson, *Proc. SPIE* **1170**, 160 (1989).

37. W. Maslach, Jr., and J. S. Sirkis, *Proc. SPIE* **1170**, 452 (1989).

38. D. W. Jensen and J. Pascual, "Degradation of Graphite/Bismaleimide," *Proc. SPIE* **1370**, 228 (1990).

39. E. H. Urruti, P. E. Blaszysk, and R. M. Hawk, *Proc. SPIE* **986**, 158 (1988).

40. J. S. Sirkis and A. Dasgupta, *Proc. SPIE* **1370**, 129 (1990).

41. C. DiFrancia, R. O. Claus, and T. C. Ward, *Proc. SPIE* **1588**, 44 (1991).

42. A. R. Raheem-Kizchery, S. B. Desu and R. O. Claus, *Proc. SPIE* **1170**, 513 (1989).

43. S. E. Baldini, D. J. Tubbs, and W. A. Stange, *Proc. SPIE* **1370**, 162 (1990).

44. A. Dasgupta, Y. Wan, J. S. Sirkis, and H. Singh, *Proc. SPIE* **1370**, 129 (1990).

45. A. M. Vengsarker, K. A. Murphy, M. F. Gunther, A. J. Plante, and R. O. Claus, *Proc. SPIE* **1588**, 2 (1991).

46. W. B. Spillman, Jr., *Proc. SPIE* **986**, 6 (1988).

47. E. Udd, ed., *Fiber Optic Sensors: An Introduction for Engineers and Scientists*. John Wiley & Sons, Inc., New York, 1991.

48. J. Dakin and B. Culshaw, eds., *Optical Fiber Sensors: Principles and Components*, Vol. 1. Artech House, Boston, 1988.

49. B. Culshaw and J. Dakin, *Optical Fiber Sensors: Systems and Applications*, Vol. 2. Artech House, Norwood, MA, 1989.

50. A. D. Kersey, in E. Udd, ed., *Fiber Optic Sensors: An Introduction for Engineers and Scientists*, John Wiley & Sons, Inc., New York, 1991.

51. B. G. Grossman, H. Hou, R. H. Nassar, A. Ren, and M. H. Thursby, *Proc. SPIE* **1370**, 205 (1990).

52. M. Thursby, K. Yoo, and B. Grossman, *Proc. SPIE* **1588**, 219 (1991).

53. B. Grossman, X. Gao, and M. Thursby, *Proc. SPIE* **1588**, 64 (1991).

54. J. M. Mazzu, S. M. Allen, and A. K. Caglayen, *Proc. Active Mater. Adaptive Struct. Conf.* Alexandria, Va., 1991, p. 243.

55. M. R. Napolitano, C. I. Chen, and R. Nutter, *Proc. Active Mater. Adaptive Struct. Conf.* Alexandria, Va., 1991, p. 247.

56. E. Udd, R. J. Michal, S. E. Higley, J. P. Theriault, P. LeCong, D. A. Jolin, and A. M. Markus, *Proc. SPIE* **838**, 162 (1987).

57. D. R. Huston, *Proc. SPIE* **1588**, 182 (1991).

58. H. Smith, Jr., A. Garrett and C. R. Saff, *Proc. SPIE* **1170**, 224 (1989).
59. E. Udd, J. P. Theriault, A. Markus, and Y. Bar-Cohen, *Proc. SPIE* **1170**, 478 (1989).
60. H. D. Simonsen, R. Paetsch, and J. R. Dunphy, *Proc. 1st Eur. Conf. Smart Struct. Mater.* Glasgow, 1992, p. 73.
61. G. Meltz, W. W. Morrey, and W. H. Glenn, *Opt. Lett.* **14**, 823 (1989).
62. W. W. Morey, *Proc. 7th Opt. Fiber Sensors Conf.* Sydney, 1990, p. 285.
63. S. M. Melle, K. Liu, and R. M. Measures, *Proc. SPIE* **1588**, 255 (1991).
64. C. E. Lee and H. F. Taylor, *Electron. Lett.* **24**, 193 (1988).
65. C. E. Lee, R. A. Atkins, and H. F. Taylor, *Opt. Lett.* **13**, 1038 (1988).
66. T. Valis, D. Hogg and R. M. Measures, *IEEE Photonics Technol. Lett.* **2**, 227 (1990).
67. C. E. Lee and H. F. Taylor, *IEEE J. Lightwave Technol.* **9**, 129 (1991).
68. C. E. Lee, H. F. Taylor, A. M. Markus, and E. Udd, *Opt. Lett.* **14**, 1225 (1989).
69. T. Valis, D. Hogg, and R. M. Measures, *Proc. SPIE*, **1370**, 154 (1990).
70. K. A. Murphy, B. R. Fogg, G. Z. Wang, A. M. Vengsarkar, and R. O. Claus, *Proc. SPIE* **1588**, 117 (1991).
71. K. A. Murphy, M. F. Gunther, A. M. Vengsarkar, and R. O. Claus, *Proc. SPIE* **1588**, 134 (1991).
72. R. J. Michal, E. Udd, and J. P. Theriault, *Proc. SPIE* 150 (1986).
73. A. D Kersey and J. P Dakin, eds., *Proc. SPIE* **1586** (1991).
74. W. B. Spillman, Jr., L. B. Maurice, J. R. Lord, and D. M. Crowne, *Proc. SPIE* **1170**, 483 (1989).
75. J. P. Dakin, D. A. J. Pearce, A. P. Strong, C. A. Wade, *Proc. SPIE* **838**, 325 (1987).
76. E. Udd, *Proc. SPIE* **1586**, 46 (1991).
77. E. Udd, ed., *Proc. SPIE, Boston, September 1988*, Vol. 986.
78. E. Udd, ed., *Proc. SPIE, Boston, September 1989*, Vol. 1170.
79. E. Udd and R. O Claus, eds., *Proc. SPIE, San Jose, September, 1990*, Vol. 1370.
80. R. O. Claus and E. Udd, eds., *Proc. SPIE, Boston, September, 1991*, Vol. 1588.
81. G. J Knowles, ed., *Proc. ADPA/AIAA/ASME/SPIE Conf.* Active Mater. Adaptive Struct. IOP, 1991.
82. B. Culshaw, P. T Gardiner, and A. McDonach, eds., *Proc. SPIE, May 1992*, Vol. 1777.
83. R. O Claus and R. S Rogowski, eds., *Proc. SPIE, September 1992*, Vol. 1798.
84. E. Udd, *Laser Focus*, 138, (May 1988).
85. R. M. Measures, *Prog. Aerosp. Sci.* **26**, 289 (1989).
86. D. A. Brown, B. Tan, and S. L. Garret, *Proc. SPIE* **1370**, 238 (1990).
87. J. A. Sirkis and H. W. Haslach, Jr., *Proc. SPIE* **1370**, 248 (1990).
88. D. R. Huston, P. L. Fuhr, P. J. Kajenski, T. P. Ambrose, and W. B. Spillman, *Proc. 1st Eur. Conf. Smart Struct. Mater.* Glasgow, 1992, p. 409.
89. H. D. Wright and R. M. Lloyd, *Proc. 1st Eur. Conf. Smart Struct. Mater.* Glasgow, 1992, p. 219.
90. A. Holst and R. Lessing, *Proc. 1st Eur. Conf. Smart Struct. Mater.* Glasgow, 1992, p. 223.
91. E. Udd, R. G. Blom, D. Tralli, E. Saaski, and R. Dokka, *SPIE Proc.* **2191**, 1994.
92. Ref. 35, 1994.

SANDRA KOSINSKI
AT&T Bell Laboratories

JOHN B. MACCHESNEY
AT&T Bell Laboratories

ERIC UDD
Blue Road Research